University of Baghdad
College of Engineering
JOURNAL OF ENGINEERING

Journal of Engineering

journal homepage: www.jcoeng.edu.iq
Number 9 Volume 24 September 2018

Mechanical and Energy Engineering

Exergy Analysis of a Domestic Refrigerator

Dr. Louay Abd Al-Azez Mahdi
Lecturer
Mechanical Engineering
University of Technology
E-mail: louayalkaesy@gmail.com

Dr. Wahid S. Mohammad*
Professor
Mechanical Engineering
University of Technology
E-mail: wahid_1953@yahoo.com

Samir Akram Mahmood
MSc. Student
Mechanical Engineering
University of Technology
E-mail: samirmc92@gmail.com

ABSTRACT

An energy and exergy thermodynamic analysis using EES program was done for a domestic refrigerator working with R-134a using vapor compression refrigeration cycle. The analysis deals with the system component, i.e. compressor, condenser, evaporator and the expansion device. The analysis depends on the entropy generation minimization approach to improve the refrigerator performance by exploring the optimum design points. These design points were derived from three different theories governing the entropy generation minimization using exergy analyzing method. These theories were first applied to find the optimum balance between the hot inner condenser area and the cold inner evaporator area of the refrigerator and between its hot and cold thermal conductances. Nine types of condensers were used according to its internal surface area and thermal conductance, in order to reach the minimum entropy generation in the refrigerator. The results showed that the compressor has the lowest exergy efficiency of 25%. The expansion device was the second component after the compressor with exergy efficiency of 92%, followed by the condenser with an efficiency of 93%. The evaporator was found to have an exergy efficiency of 98 %. The experimental tests were repeated for the nine condensers sizes with three different ambient temperatures 25°C, 30°C and 35°C. The exergy analysis showed that the design of the refrigerator mainly depends on thermal conductance calculations rather than the surface inner area estimation.

Key Words: entropy generation, exergy analysis, refrigerator.

تحليل الإكسيرجي لثلاجة منزلية

الدكتور: لؤي عبد العزيز مهدي
قسم الهندسة الميكانيكية
الجامعة التكنولوجية

الأستاذ الدكتور: وحيد شاتي محمد
قسم الهندسة الميكانيكية
الجامعة التكنولوجية

طالب الماجستير: سمير أكرم محمود
قسم الهندسة الميكانيكية
الجامعة التكنولوجية

الخلاصة

في العمل الحالي، تم إجراء تحليل حراري للطاقة والإكسيرجي باستخدام برنامج EES لثلاجة منزلية تعمل بغاز R-134a وبدورة التثليج الانضغاطية. وتناول التحليل مكونات النظام، أي الضاغط والمكثف والمبخر وأداة الخنق. وأعتمد التحليل على نهج تقليل توليد الإنتروبي. أجريت هذه الدراسة لتحسين أداء الثلاجة واستكشاف نقاط التصميم الأمثل لها. وقد استمدت نقاط التصميم هذه من ثلاثة نظريات مختلفة تحكم تقليل توليد الإنتروبي باستخدام نهج تحليل الإكسيرجي. تم تطبيق هذه النظريات أولاً للحصول على التوازن الأمثل بين منطقتي المكثف الداخلية الساخنة والمبخر الداخلية الباردة في الثلاجة وبين الايصالية

*Corresponding author
Peer review under the responsibility of University of Baghdad.
https://doi.org/10.31026/j.eng.2018.09.01

Article accepted: 28/11/2017

الحرارية الساخنة والباردة. وتم استخدام تسعة أنواع من المكثفات وفقاً لمساحتها الداخلية السطحية والايصالية الحرارية، من أجل الوصول إلى الحد الأدنى من توليد الإنتروبي في الثلاجة. أظهرت النتائج أن الضاغط لديه أقل كفاءة إكسيرجي وكانت 25%. وكانت أداة الخنق المكون الثاني بعد الضاغط مع كفاءة إكسيرجي 92%، يليه المكثف بكفاءة 93%. اما كفاءة الإكسيرجي للمبخر كانت 98%. تم تكرار الاختبارات العملية لأحجام المكثف التسعة لثلاث درجات حرارة سيليزية محيطية مختلفة 25، 30 و35. أظهر تحليل الإكسيرجي أن تصميم الثلاجة يعتمد أساساً على حسابات الايصالية الحرارية، وليس على المساحة السطحية الداخلية المخمنة.

الكلمات الرئيسية: توليد الانتروبي، تحليل الاكسيرجي، الثلاجة.

1. INTRODUCTION

Refrigeration occupies a wide range in domestic and commercial sectors for cooling and food preservation applications. This causes an increase in energy demand, which requires an efficient energy utilization for useful application. One of its applications is the domestic refrigerator, which is now used in every house in the world. The design and optimization of the domestic refrigerator is an initial issue in reducing energy consumption and therefore reducing electricity bill of the household. Condensers and evaporators inner area represent governing parameters in designing the domestic refrigerator. The effect of these parameters is to be tested experimentally and analyzed theoretically using the entropy generation minimization approach. These tests are to be repeated for three environmental temperatures 25℃, 30℃ and 35℃ applied to 10-ft^3 domestic refrigerator working with R134a to optimize its performance. Several sizes of the condenser are to be considered.

The refrigeration system performance can be evaluated using energy and exergy analysis, which are based on the first and second law of thermodynamics. The researchers have given a pronounce physical reasoning for the losses and its percentage in the refrigerator, in order to improve the performance.

Bejan, 1989 carried out a theoretical analysis of refrigeration system. Two arguments were explained, the first was based on a refrigeration plant model, the irreversibility of which is due solely to the internal heat transfer that passes directly through the machine all the way to the load temperature. The second argument was based on a more refined model in which the refrigeration plant irreversibility is due to three heat transfer phenomena. It was shown that there exist optimum ways of allocating heat transfer equipment to the distinct parts of the plants, to make a balance between the hot and cold end heat exchangers in the refrigeration plant. **Klein,** and **Reindl, 1998** investigated theoretically the effect of heat exchanger allocation on overall system performance and entropy generation rate using both reverse Carnot and vapor compression refrigeration cycle models. The vapor compression model considers non-ideal compressor performance, compressor volumetric efficiency, refrigerant properties, and throttling in addition to mechanistic heat exchanger models. The results support the conclusions of, **Bejan, 1989,** that maximum performance is observed when the condenser and evaporator sizes are approximately equal. **Chang, 2006** developed a theoretical investigation on the optimal design of a refrigeration plant with considerations on both external and internal irreversibilities. The optimal area-ratio and the corresponding maximum coefficient of performance solutions have more significant effects on a freezing system than on an air-conditioning system. For the case of no internal irreversibility, the analytical solution gave a similar results to that of, **Bejan, 1989** and, **Klein,** and **Reindl, 1998**. **Stanciu et al., 2011** performed a comparative theoretical exergy analysis on the operation and performances of one stage vapor compression refrigeration system using several refrigerants R22, R134a, R717, R507a and R404a. The investigation gave a suitable indication on the compression ratio, superheating of the cycle and exergy destruction rates. **Ukey,** and **Chaudhary, 2012** used a theoretical exergy analysis for a domestic refrigerator working with R134a and R12. The analysis showed that the cooling load and the second law efficiency were affected by the change in evaporator and condenser temperatures. Also the dead-

state temperature, which is varying, according to the particular geological location of the system affects the second law efficiency. **Roy, and Mandal, 2014** made a theoretical analysis for an ideal vapor compression refrigeration system using different refrigerants R12, R134a and R290 and developed a mathematical model to solve the mathematical problems. Various parameters was computed which included compressor power, coefficient of performance of the system, total exergy loss, mass flow rate and exergy efficiency. The analysis found that the compressor power increases with decrease in evaporator temperature and increase in condenser temperature for all three refrigerants. Exergy loss of the system increases with the decrease in evaporator temperature. **Khan, et al., 2015** provided a detailed exergy analysis for theoretical vapor compression refrigeration cycle using R12, R22 and R134a. The equations of exergetic efficiency and exergy destruction for the main system components such as compressor, condenser expansion device and evaporator were developed. It was found that exergy efficiency and COP increases with increase in degree of subcooling for all refrigerants. **Prakash, et al., 2016** presented a theoretical energetic and exergetic performance of vapor compression refrigeration system working with mixture of refrigerants to replace R12. A computational model was produced based on this analysis solved using MATLAB for the effects of evaporator temperatures on exergy efficiency, and exergy defect on coefficient of performance. They found that the highest irreversibility was in the compressor followed by the evaporator, the expansion valve and the condenser.

Most of these studies focused on analyzing each component in the system separately to show its efficiency. In the present study, the theoretical entropy generation minimization approach is to be applied to experimental results to obtain the optimum design point between the condenser and evaporator of a 10 ft^3 domestic refrigerator in terms of inner areas and overall heat transfer coefficient. These tests are to be repeated for three ambient temperatures 25°C, 30°C and 35°C in an isolated and controlled environment. Nine different sizes of the condenser tube are to be used to carry out the experimental tests.

2. DOMESTIC REFRIGERATOR

The Domestic Refrigerator consists of a cabinet, an evaporator, a compressor, a condenser and a capillary tube. The refrigerator is made of a pressed steel with paint and waterproof outside shell. Expanded polyurethane panels are installed between the outer and the inner shells to minimize heat gain. The specifications of the main components are as follows; the compressor: hermetic reciprocating one manufactured by Danfoss Company model: FR6G. The condenser: is a static condenser (wire on the tube), which exchange heat by natural convection and radiation with the environment. The evaporator is a roll-bond two-layered evaporator panel with symmetrical channels on both sides. The capillary tube is a copper capillary tube type. It was selected using selection software according to ASHRAE technical committee 8.9, **ASHRAE, 1997**. The refrigerator cabinet is made of pressed steel with white paint. Polyurethane foam filled the space between the outer and inner plastic shell to minimize heat transfer losses from the cabinet to the outside, and maintain the refrigerated space at a constant temperature.

3. INSTRUMENTATION

Several measuring instruments have been used with domestic refrigerator. Thermistors of negative temperature coefficient (NTC) type are used to measure the temperature. The pressure gauges were used to indicate the pressure at high and low-pressure sides of the refrigerant circuit. Also, four pressure transducers were used to measure the pressure across the compression cycle of the domestic refrigerator. A turbine refrigerant mass flow meter made from stainless steel was used to measure the flow rate of refrigerant. Digital power clamp meter was used to

measure the current, the voltage supplied to the refrigerator and the power consumption per hour and day. All measuring devices are connected with interface unit Data Acquisition DAQ. The interface Arduino connected to the computer control system (Laptop) in order to view the data using LABVIEW software, which enables the communication between the systems under study. The rig is modified according to the need for carrying up exergy analysis to each component in the vapor compression refrigeration system. After the system modifications were accomplished, leak checking is required to assure that there is no leak in the system. The refrigerant was charged using refrigerant R134a can and an electronic scale to measure the required amount of refrigerant mass.

4. THERMODYNAMIC MODEL

The thermodynamic model for a domestic refrigerator is done according to the basis of the most recent method that has a novel idea. The vapor compression refrigeration cycle consists of four thermodynamic processes**:** 1-2 suction line, 2-3 isentropic compression, 3-4 discharge line, 4-5 heat rejection, 5-6 isenthalpic throttling, 6-1 heat absorption as shown in **Fig. 1**. Several effects have a major impact on the cycle due to the irreversible processes. The first one is friction losses and heat losses in the compressor. Others are pressure drop in the heat exchangers and connecting lines, the superheating at evaporator outlet, heat transfer from the refrigerant to the air depends on the heat exchanger effectiveness and the superheat and sub-cool the refrigerant in the system. The cycle elements are modeled as follows:

4.1 Compressor

The modeling of the thermal performance of a household hermetic reciprocating compressor depends on thermal analysis to find the total power input, and mass flow rate. The second is to find the approximate properties of the outlet refrigerant, which lead to the calculation of the power required to compress the refrigerant. The power input to the compressor is the summation of the work and the power required to overcome the friction and heat losses, which can be expressed in the form, **Bejan, 1996** and**, Bejan, 2006**:

$$P = W + Q_{total\ losses} \quad (1)$$

$$W = \dot{m}_r * (h_3 - h_2) \quad (2)$$

$$Q_{total\ losses} = Q_{conv\&rad\ losses} + Q_{friction\ losses} \quad (3)$$

$$Q_{convlosses} = \alpha_{comp} * A_{scomp} * (T_{shell} - T_{amb}) \quad (4)$$

To find the heat transfer coefficient, the relations of the vertical cylinder will be used as follows:

$$Nu = c * Ra^m \quad (5)$$

$$Nu = \frac{\alpha_{comp} * L_c}{K_a} \quad (6)$$

$$Ra = \frac{g * \beta * (T_{shell} - T_{amb}) * \rho_a^2 * Lc^3}{\mu^2} \quad (7)$$

Where $Lc = \frac{A_{scomp}}{Perimeter}$, $\beta = \frac{1}{T_{film}}$, and $T_{film} = \frac{T_{shell} + T_{amb}}{2}$

All properties are taken at T_{film}.

The radiation heat transfer losses from the compressor shell, which has an important percentage compared to the natural convection losses, can be calculated as:

$$Q_{radlosses} = F_{1-2} * \sigma_B * A_{scomp} * \epsilon_{scomp} * (T_{shell}^4 - T_{amb}^4) \quad (8)$$

The exergy analysis of an energy balance is required such as:

$$Power - \dot{m}_r * \sum_{in} h_2 = \dot{m}_r * \sum_{out} h_3 + Q_{total\ losses} \quad (9)$$

$$ED_{comp} = \left(1 - \frac{T_{amb}}{T_{shell}}\right) Q_{total\ losses} - Power + \sum_{in} ex - \sum_{out} ex \quad (10)$$

$$\zeta_{comp} = \frac{ED_{comp}}{Power} \quad (11)$$

and the exergy efficiency: $\eta_{\Pi,\text{comp}} = \eta_{ex.comp} = 1 - \zeta_{comp}$ (12)

4.2 Wire Condenser

The wire condenser is used to reject the heat of the refrigerant to the air. This type of condenser usually means poorer heat exchanger and therefore more contribution of external and internal losses. The following assumptions are considered: Steady-state case and one-dimensional analysis. Cross flow heat exchanger, iron tubes, bends, and iron fins, unmixed refrigerant side and mixed airside. The refrigerant side is divided into three regions, superheat, two-phase, and subcooled. The bends have an effect on the heat transfer in the three regions. The two-phase region for the refrigerant is considered homogenous mixture. The effects of the kinetic and potential energies of the refrigerant are negligible. Properties of the refrigerants are uniform thermodynamically. Smooth tube type for inside, and outside. There is no change in the temperature and pressure of the refrigerant with the radius of the tube. A linear relation between heat transfer coefficient and pressure drop with the quality. Using Muller-Stenhagan correlation for pressure drop in the two-phase flow.

4.2.1 Refrigerant Side

The three regions of superheat, subcooled and two-phase flow are considered subsequently.

4.2.1.1 Superheat and subcooled regions:

The superheat region is the first part of the condenser and the refrigerant in gas phase while the subcooled region is the last part of the condenser and the refrigerant in the liquid phase. The heat transfer coefficient can be determined according to the following correlations, **Incropera, et al., 2010**.:

$$St \cdot Pr^{\frac{3}{2}} = a \cdot Re^{b} \quad (13)$$

The properties are evaluated at the film temperature, T_{film}.

$$T_{film} = \frac{T_{wall}+T_{bulk}}{2}$$

In Eq. (13) a, b are constants with values shown in **Table 1.**

The heat rejected is given by:

$$Q_{4-sat} = \dot{m}_r cp_4 * (T_4 - T_{cin-sat}) \quad (14)$$

$$Q_{4-sat} = \alpha_{4-sat} * A_{si-4} * (T_{4-csat} - T_{wi-4csat}) \quad (15)$$

Where:

$A_{si-4} = \pi \cdot d_i \cdot L_{superheat}$

$L_{superheat} = \frac{\pi.d_i}{A_{si-4}}$

$T_{cin-sat}$ = Refrigerant temperature at inlet saturated region.

$T_{4-csat} = (T_4 + T_{cin-sat})/2$ is the average temperature of the refrigerant at inlet and outlet at the superheat region.

$T_{wi-4csat} = (T_{wi} + T_{cin-sat})/2$ is the average temperature of inside tube wall at the inlet and outlet at the superheat region.

The total pressure drop is the summation of the friction pressure drop and the momentum pressure drop as well as the gravity pressure drop that is neglected.

The total pressure drop is the summation of the friction, momentum, and bends pressure drop.

$$\Delta P_{total} = \Delta P_{friction} + \Delta P_{mom} + \Delta P_{bends} \quad (16)$$

4.2.1.2 Two phase region:

It is the second part of the condenser, which covers more than 85% of total area of the condenser, **ASHRAE, 1997**. The heat transfer rate can be calculated by:

$$Q_{two-phase} = \dot{m}_r * h_{fg} \quad (17)$$

The target is to find the suitable two-phase area in order to reject this heat. The first step is to find the type of flow pattern in order to calculate the heat transfer coefficient, the two-phase flow may be stratified, stratified wavy, bubbly and mist flow. To identify the flow pattern at a particular value of vapor quality x, the following limitations are to be applied, **Hajal, et al., 2003** and**, Thome, et al., 2003**:

- Annular flow exists if $G > G_{wavy},\ G < G_{mist}\ and\ x > x_{IA}$.
- Intermittent flow exists if $G > G_{wavy},\ G < G_{mist}\ or\ G < G_{bubbly}\ \ and\ x < x_{IA}$.
- Stratified-wavy flow exists if $G_{strat} < G < G_{wavy}$;
- Fully stratified flow exists if $G < G_{strat}$.
- Mist flow exists if $G > G_{mist}$.

The heat transfer coefficient is given by, **Thome, et al., 2003**:

$$\alpha_{ctp} = \frac{\alpha_f * \frac{D_{ci}}{2} * \theta + [2*\pi - \theta] * \frac{D_{ci}}{2} * \alpha_c}{2*\pi*\frac{D_{ci}}{2}} \quad (18)$$

Following **Traviss, 1972,** the energy balance was used to calculate the two-phase length.

The important point is the length of the two-phase area, the diameter is fixed as 6.35mm (1/4)″, with an inner diameter of 4.42mm, so the area is the target.

The approximate length can be found from the relation of the energy balance, **Traviss, 1972** as follows:

$$\alpha_{ctp} * A_{s-tp} * \Delta T = \dot{m}_r * h_{fg} * \Delta x \quad (19)$$

$G = \frac{\dot{m}_r}{A_c}$ and $A_c = \pi * D_{ci}^2/4$

$$\alpha_{ctp} * \pi * d_i * l * \Delta T = G * \frac{\pi * d_i^2}{4} * h_{fg} * \Delta x$$

Let $l = dz\ and\ \Delta x = dx$

Re-arrangement yields:

$$\frac{dz}{dx} = \frac{G * h_{fg} * d_i}{4 * \alpha_{ctp} * \Delta T}$$

$$\int dz = \frac{G * h_{fg} * d_i}{4 * \alpha_{ctp} * \Delta T} \int dx$$

It is the length of the tube is required to cover the change in the quality, and the average heat transfer coefficient can be found from the following:

$\frac{1}{\alpha_{ctp}} = \frac{1}{x_i - x_e} \int_{xe}^{xi} \frac{dx}{dz}$ This expression is a function for quality only.

$$Q_{two-phase} = \alpha_{ctp} \cdot A_{i-tp} \cdot (T_R - T_{win}) \quad (20)$$

From equation (20), the length of the two-phase region will be found.

The flow pattern will be determined according to Cavallini limitations, where the total pressure drop in the saturated region is the summation of pressure drop due to, friction, momentum. The gravity pressure drop is the horizontal layout of the tubes will be neglected.

$$\Delta P_{tp-total} = \Delta P_{tp-friction} + \Delta P_{tp-mom} + \Delta P_{tp-bends} \quad (21)$$

4.2.2 Air Side:

The condenser shape and configuration allow a good understanding of the behavior of the heat

transfer and the pressure drop. Before clarifying the analysis of the condenser airside, the fin efficiency, the finned tube surface effectiveness, the overall heat transfer coefficient, and the Ɛ-NTU method should be determined as follows:

The actual fin efficiency is calculated using the approximation for fin geometry relation:

$$\eta_f = \frac{tanh(m \cdot L)}{m \cdot L} \quad (22)$$

Where:

$$m = \sqrt{\frac{4 \cdot \alpha_{air}}{K_{fin} \cdot D_f}}$$

The finned tube surface is described using its areas, where:

$$A_{tot} = A_f + A_t \quad (23)$$

$$A_f = \pi * D_f * L_f * No.fins - A_{contact} \quad (24)$$

$$A_{tube} = \pi * D_{to} * L_{tube} - A_{contact} \quad (25)$$

$$A_{contact} = \left(D_f * D_{to} * 0.75\right) * No.legs * No.fins \quad (26)$$

To calculate the heat transfer by natural convection and radiation the following steps to be applied:

The natural convection heat transfer coefficient is divided according to surfaces horizontal and vertical:

The heat transfer coefficient for horizontal surfaces α_{cah} equations.

$$Ra_h = \frac{9.81 * \beta * [T_{cs} - T_{amb}] * Dc_o^3 * Pr_a}{\left[\frac{\mu_a}{\rho_a}\right]^2} \quad (27)$$

If $[Ra_h < 10^9]$

$$\alpha_{cah} = 1.32 * \left[\frac{T_{cs} - T_{amb}}{Dc_o}\right]^{0.25} \quad (28)$$

If $[Ra_h > 10^9]$

$$\alpha_{cah} = 1.52 * [T_{cs} - T_{amb}]^{0.3333} \quad (29)$$

The heat transfer coefficient for vertical surfaces α_{cav} equations.

$$Ra_v = \frac{9.81 * \beta * [T_{cs} - T_{amb}] * H_c^3 * Pr_a}{\left[\frac{\mu_a}{\rho_a}\right]^2} \quad (30)$$

If $[Ra_h < 10^9]$

$$\alpha_{cav} = 1.42 * \left[\frac{T_{cs} - T_{amb}}{H_c}\right]^{0.25} \quad (31)$$

If $[Ra_h > 10^9]$

$$\alpha_{cav} = 1.31 * [T_{cs} - T_{amb}]^{0.3333} \quad (32)$$

The radiation heat transfer coefficient α_{crad}:

$$\alpha_{crad} = \epsilon * 5.67 * 10^{-8} * \left[\frac{(T_{cs})^4 - (T_{amb})^4}{T_{cs} - T_{amb}}\right] \quad (33)$$

To calculate the wire fin efficiency:

$$k_{iron} = 72.9 * e^{[-0.0008166 * T_{cs}]}$$

$$m_{fin} = \left[\frac{4 * (\alpha_{cav} + \alpha_{crad})}{k_{iron} * D_f}\right]^{0.5} \quad (34)$$

$$\eta_{fin} = \frac{\tan h[m_{fin} * L_{fin}]}{m_{fin} * L_{fin}} \quad (35)$$

To calculate the surface efficiency:

$$\eta_s = 1 - \frac{A_f}{A_{tot}}\left(1 - \eta_f\right) \quad (36)$$

The heat transfer from the wire condenser:

$$Q_{fin} = [\alpha_{cav} + \alpha_{crad}] * A_w * [T_{cs} - T_{amb}] * \eta_{fin} \quad (37)$$
$$Q_{tube} = [\alpha_{cah} + \alpha_{crad}] * A_{tube} * [T_{cs} - T_{amb}] \quad (38)$$
$$Q_{ctotal} = Q_{fin} + Q_{tube} \quad (39)$$
$$R_{oc} = \frac{1}{[\alpha_{cav}+\alpha_{crad}]*A_{tube}*\eta_{cond}} \quad (40)$$

The overall heat transfer coefficient is determined by the following equation:

$$\frac{1}{UA} = \frac{1}{\eta_s \cdot \alpha_{ac} \cdot A_{tot}} + \frac{\ln\frac{r_o}{r_i}}{2\pi . K_p . l_p} + \frac{1}{\alpha_{icave} \cdot A_i} \quad (41)$$

The effect of fouling inside and outside is neglected because the refrigerator is brand new.
The effectiveness of the wire condenser is calculated by considering the heat exchanger unmixed-mixed cross-flow configuration, **Incropera, et al., 2010 and, Holman, 2010**:

$$\mathcal{E}_{H.E} = 1 - \exp\{-(1/C^*) \cdot [1 - exp(-NTU \cdot C^*)]\} \quad (42)$$

Where:

$C^* = \frac{C_{min}}{C_{max}}$ where $C = \dot{m} * C_p$

Also $\mathcal{E}_{H.E}$ can be defined as:

$$\mathcal{E}_{H.E} = \frac{Q_{act}}{Q_{max}} = \frac{\dot{m} \cdot C_{min} \cdot (T_{ci} - T_{co})}{\dot{m} \cdot C_{min} \cdot (T_{hi} - T_{ci})} \text{ Which leads to } \mathcal{E}_{H.E} = \frac{(T_{ci} - T_{co})}{(T_{hi} - T_{ci})} \quad (43)$$

$$NTU = \frac{UA}{C_{min}} \quad (44)$$

NTU determines the 'thermal size' of a heat exchange, which will be calculated from equation (42).

4.2.3 Exergy analysis of the condenser:

The condenser represents the second component in the vapor compression refrigeration system. The condenser was made of iron tube and fins printed with black color.

The energy:

$$\dot{m}_r \cdot h_4 + \dot{m}_a \cdot \alpha_{ainc} = \dot{m}_r \cdot h_5 + \dot{m}_a \cdot h_{aoutc} + Q_{cond\ losses} \quad (45)$$
$$Q_{cond\ losses} = \dot{m}_r \cdot (h_4 - h_5) - \dot{m}_a \cdot (h_{ainc} - h_{aoutc}) \quad (46)$$

The exergy analysis:

$$ED_{cond} = \left(1 - \frac{T_{amb}}{T_{wallcond}}\right) Q_{lossescond} + \sum_{in} ex - \sum_{out} ex$$

Where:

$$\sum_{in} ex = \dot{m}_r \cdot \left(ex_4 + \frac{P_{4rcond}}{\rho_4}\right) + \dot{m}_a \cdot \left(ex_{ainc} + \frac{P_{ainc}}{\rho_{ain}}\right)$$
$$\sum_{out} ex = \dot{m}_r \cdot \left(ex_5 + \frac{P_{5rcond}}{\rho_5}\right) + \dot{m}_a \cdot \left(ex_{aoutc} + \frac{P_{aoutc}}{\rho_{aout}}\right)$$

The final form for the exergy analysis is:

$$ED_{cond} = \left(1 - \frac{T_o}{T_{wallcond}}\right) Q_{lossescond} + \dot{m}_r \cdot \left[(ex_4 - ex_5) + \frac{\Delta P_{45cond}}{\rho_4}\right] + \dot{m}_a \cdot (ex_{ainc} - ex_{aoutc}) \quad (47)$$

$$\zeta_{cond} = \frac{ED_{cond}}{Power_{total}} \quad (48)$$

The exergy efficiency is given by: $\eta_{cond} = 1 - \zeta_{cond}$ (49)

4.3 Throttling Device

The throttling device is the controller of refrigerant mass flow rate and to keep the pressure

difference between the high side and low side. The capillary tube is used, as a throttling device due to low cost, but it is not sensitive to the deviation that happens to the system due to the effect of environment.

The assumptions for throttling device are Fixed capillary tube area. Constant flow rate. Isenthalpic expansion. Subcooled inlet refrigerant temperature. Entropy generation due to pressure drop is more than that for heat transfer.

From the energy balance got a throttling process only from the steady state thermodynamic equation, because no work suspended or heat loss is added to the valve system.

$$h_5 = h_6 \tag{50}$$

The exergy destruction:

$$ED_{throttling} = \left(1 - \frac{T_o}{T_w}\right) Q_5^6 + \dot{m}_r \cdot \sum_{in} \left[ex_5 + \frac{P_5}{\rho_5}\right] - \dot{m}_r \cdot \sum_{out} \left[ex_6 + \frac{P_6}{\rho_6}\right]$$

$$ex_5 = (h_5 - h_o) - T_o \cdot (s_5 - s_o)$$

$$ex_6 = (h_6 - h_o) - T_o \cdot (s_6 - s_o)$$

Since, $\left(1 - \frac{T_o}{T_w}\right) Q_5^6 = 0$ and $W = 0$

Then the final form is given as:

$$ED_{throttling} = \dot{m}_r * \left[\left(T_o \cdot (s_6 - s_5)\right) + \frac{\Delta P_{56}}{\rho_5}\right] , \tag{51}$$

$$\zeta_{throttling} = \frac{ED_{throttling}}{Power_{total}} \tag{52}$$

The exergy efficiency is: $\eta_{throttling} = 1 - \zeta_{throttling}$ (53)

4.4 Evaporator

The fourth important part of the vapor compression refrigeration system is the evaporator. The following assumptions are considered in the modeling of the evaporator: Steady state, one-dimensional analysis. Natural convection heat transfer. Roll bond heat exchanger of aluminum covered with thermal paint, the inner side refrigerant is mixed flow due to the shape of the passages, and the air is mixed also. The inside and outside tube surfaces are of the smooth types. Properties for refrigerants are uniform thermodynamically. The refrigerant side is divided into two regions, saturated and superheat. The saturated region for the refrigerant side is considered homogenous mixture, and the nucleate boiling and convection boiling happen at the same time. The effect of the kinetic and potential energy of the refrigerant is negligible. The total length of the inside area is constant. A linear relation between the pressure and quality for the refrigerant at two-phase Region. The heat transfer for air happens for dry surface only and by natural convection and radiation.

4.4.1 Refrigerant side:

The saturated region covers more than 80% of the total area of the evaporator. The **Kandlikar, 1990** correlation for a saturated two-phase flow boiling heat transfer inside horizontal and vertical tubes are used in order to calculate the local heat transfer coefficient inside the evaporator tubes.

$$\frac{\alpha_{tpevap}}{\alpha_l} = C_1 \cdot C_o^{c2} \cdot (25Fr_{lo})^{c5} + C_3 \cdot B_o^{c4} \cdot F_{fl} \tag{54}$$

The first term represents the convective boiling and the second term represents the nucleate boiling. The single-phase liquid heat transfer coefficient will be calculated by Dittus-Boelter correlation:

$$\alpha_l = 0.023 \cdot Re_l^{0.8} \cdot Pr_l^{0.4} \cdot \left(\frac{k_l}{D_{ei}}\right) \tag{55}$$

Where:

$Re_l = \frac{G*[1-x1]*D_{ei}}{\mu_l}$

$C_o = \left(\frac{1-x}{x}\right)^{0.8}\left(\frac{\rho_V}{\rho_L}\right)^{0.5}$ Convection number.

$B_o = \frac{q}{Gi_{lg}}$ Boiling number.

$Fr_{lo} = \frac{G^2}{\rho_l^2 gD}$ Froude number with all flow as liquid.

$C_1 = 1.136, C_2 = -0.9, C_3 = 667.2, C_4 = 0.7, C_5 = 0.3$ are constants.

The convection-boiling region happens at a convection boiling number Co < 0.65 while the nucleate boiling is done at Co> 0.65. For a vertical and horizontal flow with Fr_{lo} > 0.04, the Froude number multiplier in the convection boiling term becomes unity. The fluid dependent parameter $F_{fl} = 1.5$ for R12, which is the nearest refrigerant to R134a.

By using the same method in the condenser, the average heat transfer and the tube length will be found.

$$\alpha_{avee} = \frac{\alpha_{etpave}*A_{ei}*RQ_{sat}+\alpha_{she}*A_{ei}*RQ_{super}}{A_{ei}} \quad (56)$$

Where: $= \frac{1}{\alpha_{avee}*A_{ei}}$, $RQ_{sat} = \frac{\delta_{hsat}}{\delta_{htot}}$, $RQ_{super} = \frac{\delta_{hsuper}}{\delta_{htot}}$

The pressure drop in this region is similar to that detailed in the condenser section.

The second region of the evaporator is the superheat region, which covers less than 20% of the total area. The heat transfer coefficient and the pressure drop will be found by the same correlations used in the superheat region for the condenser.

.

4.4.2 Airside:

In order to calculate convection and radiation heat transfer coefficients of the outer surface of the evaporator, it was split into eight areas. Four vertical areas and four horizontal areas according to the face direction heat transfer.

The radiation heat transfer coefficient α_{erad}:

$$\alpha_{crad} = \epsilon * 5.67 * 10^{-8} * \left[\frac{(T_{ae})^4-(T_{we})^4}{T_{ae}-T_{we}}\right] \quad (57)$$

The convection heat transfer for vertical surfaces was calculated as follows, **Incropera, et al., 2010**:

$$\overline{Nu}_L = \left\{0.825 + \frac{0.387Ra_L^{1/6}}{\left[1+(0.492/Pr)^{9/16}\right]^{8/27}}\right\}^2 = \frac{\alpha_{eav}L_c}{K_a} \quad (58)$$

$L_c = \frac{A_{sv}}{P}$

$$Q_{conv1} = 4 * A_{vs} * [\alpha_{eav} + \alpha_{erad}] * (T_w - T_{ae}) \quad (59)$$

The convection heat transfer for horizontal surfaces was calculated as following, **Incropera, et al., 2010**:

For lower surface:

$$\overline{Nu}_L = 0.54Ra_L^{1/4} \qquad 10^4 \le Ra_L \le 10^7 \quad (60)$$

$$\overline{Nu}_L = 0.15Ra_L^{1/3} \qquad 10^7 \le Ra_L \le 10^{11} \quad (61)$$

$$Q_{conv2} = 2 * A_{hs} * [\alpha_{eah} + \alpha_{erad}] * (T_w - T_{ae}) \quad (62)$$

Upper surface:

$$\overline{Nu}_L = 0.27Ra_L^{1/4} \qquad 10^5 \le Ra_L \le 10^{16} \quad (63)$$

$$Q_{conv3} = 2 * A_{hs} * [\alpha_{eah} + \alpha_{erad}] * (T_w - T_{ae}) \quad (64)$$

$$Q_{ea} = Q_{conv1} + Q_{conv2} + Q_{conv3}$$
$$\alpha_{eaave} = \frac{4*A_{vs}*[\alpha_{eav}+\alpha_{erad}]+2*A_{hs}*[\alpha_{eah}+\alpha_{erad}]+2*A_{hs}*[\alpha_{eah}+\alpha_{erad}]}{A_{esot}} \quad (65)$$
$$Roe = \frac{1}{\alpha_{eaave}*A_{esot}}$$
$$Retot = Rie + Roe$$
$$UAe = \frac{1}{Retot}$$
$Where$: $A_{hs1} = A_{hs3} = 0.09394m^2$ the horizontal outer surface area
$A_{vs2} = A_{vs4} = 0.05135m^2$ the vertical outer surface area

4.4.3 Exergy analysis of the evaporator:
The energy balance is given as:
$$\dot{m}_r \cdot h_6 + \dot{m}_a \cdot h_{aine} = \dot{m}_r \cdot h_1 + \dot{m}_a \cdot h_{aoute} + Q_{evap\ losses}$$
$$Q_{evap\ losses} = \dot{m}_r \cdot (h_6 - h_1) - \dot{m}_{aevap} \cdot \left(h_{ainevap} - h_{aoutevap}\right) \quad (66)$$
The exergy balance is given as:
$$ED_{evap} = \left(1 - \frac{T_{ae}}{T_{wallevap}}\right) Q_{lossesevap} + \sum_{in} ex - \sum_{out} ex$$
The final form for the exergy analysis is:
$$ED_{evap} = \left(1 - \frac{T_{ae}}{T_{wallevap}}\right) Q_{lossesevap} + \dot{m}_r \cdot \left[(ex_6 - ex_1) + \frac{\Delta P_{61cond}}{\rho_6}\right] + \dot{m}_a \cdot \left[(ex_{aine} - ex_{aoute}) + \frac{\Delta P_{aevap}}{\rho_{ainevap}}\right] \quad (67)$$

The exergy destruction of air will be neglected due to the smallest value.

$$\zeta_{evap} = \frac{ED_{evap}}{Power_{total}} \quad (68)$$

The exergy efficiency is given by: $\eta_{\Pi,evap} = 1 - \zeta_{evap}$ (69)

The analysis and the optimization of the refrigerator were carried out using EES software.

5. RESULTS AND DISCUSSION:

A number of legs in the figures represent the condensers sizes.

Figs. 2 and 3 show the T-s and P-h diagrams of the vapor compression refrigeration cycle for different sizes of condensers at 25℃ ambient temperature. The compressor compression ratio remained constant, which means that the compression ratio does not affect the increase in condenser size. The condenser and evaporator pressures and temperatures decrease with the increase in the condenser size. The dryness fraction decreases with the increase in the condenser size, which gives a better cooling effect in the evaporator side due to the increase in the cooling effect. The maximum and minimum temperatures of each cycle are shifted down with the increase in the condenser size. That is happening due to the drop in the pressure, which leads to a drop in the condenser and evaporator temperatures. The T-s diagram and P-h diagram are for the same system working at ambient temperatures 30℃ and 35℃ and the same behavior were seen.

Figs. 4 and 5 show the T-s and P-h diagrams of the vapor compression refrigeration cycle for 15 legs condenser at different ambient temperature 25℃, 30℃ and 35℃. The compression ratio remained the same despite the change in the suction and discharge pressure and temperature. The condenser and evaporator temperature increases with the increase in the ambient temperature. The dryness fraction increases with the increase in the ambient temperature, which acts to

decrease the cooling effect. The cycle maximum and minimum pressure shift up with the increase of the ambient temperature. The two-horn area is increased with the increase in the ambient temperature that means an increase in the compressor losses and the inlet of the evaporator, which reduced the cooling effect.

Fig. 6 shows the relation between the subcooled degrees with different sizes of condensers at 25℃, 30℃ and 35℃ ambient temperatures. The degree of subcooled increases gradually with the increase in the condenser size at different ambient temperature.

Fig. 7 shows the relation between the evaporator wall temperatures with different sizes of condensers at different ambient temperatures 25℃, 30℃ and 35℃. The value of evaporator wall temperature decreases with the increase in the condenser size at each of the ambient temperature, due to the increase in the amount of liquid refrigerant that passes to the evaporator leading to temperature reduction.

Fig. 8 shows the relation between the compressor surface temperatures with different sizes of condensers at different ambient temperatures 25℃, 30℃ and 35℃. The value of compressor surface temperature decreases from 71.6℃ to 58℃, with the increase in the condenser size at each ambient temperature. This decrease is due to the low suction temperature.

Fig. 9 shows the relation between the mass velocities with different sizes of the condenser at different ambient temperatures 25℃, 30℃ and 35℃. The value of mass velocity increases with the increase in the condenser size at each ambient temperature, with a range from 56 kg/m^2 to 66kg/m^2. That is due to the increase in the refrigerant mass inventory.

Fig. 10 shows the relation between the power consumption with different sizes of the condenser at different ambient temperatures 25℃, 30℃ and 35℃. The power increases with the increase in the condenser size at each ambient temperature, with a range from 157W to 206W. That also happens due to the increase in refrigerant mass inventory.

Fig. 11 shows the relation between the total power consumption and the losses with different sizes of condensers at 25℃ ambient temperature. The figure shows that the power consumption increases gradually with the increase in condensers sizes. The increase in the power done due to the increase in refrigerant mass inventory. The total losses took 2/3 of the power consumption, which included the convection losses, radiation and friction losses. The convection and radiation losses seem to remain constant with different sizes of condensers and the radiation losses are larger than the convection losses. The friction losses increase with the increase in the wire condenser size. It is lower than the convection and radiation losses till 17 legs condenser after that the friction is the greater. The actual work took 1/3 of the total power consumption, which means that the compressor works in the worst condition due to the largest losses. This highlighted the critical area that needs more research to improve the behavior of the household compressor.

The power consumption and the losses for 30℃ and 35℃ ambient temperatures are the same as shown in **Fig. 11.**

Fig. 12 shows the relation between the compressor exergy with different sizes of condensers at 25℃, 30℃ and 35℃ ambient temperatures. The figure refers to the place where the condenser and evaporator heat capacities UA at 13 legs condenser are equal. The other point where the internal surface areas are equal is at 26 legs condenser. The exergy behavior of the compressor at each ambient temperature is the same and it is increased till condensers legs 13 to 15, after that the exergy drop down. The maximum exergy is 26 % at condenser with legs between 13 to 15, which refers to the best operation points.

Fig. 13 shows the relation between the condenser exergy with different sizes of condensers at different ambient temperatures 25℃, 30℃ and 35℃. The condenser exergy efficiency value is

ranging between (88-96) %. This higher condenser exergy value was due to the low-pressure drop and the small difference in the inlet and outlet refrigerant temperature across the condenser.
Fig. 14 shows the relation between the throttling exergy with different sizes of condensers at different ambient temperatures 25℃, 30℃ and 35℃. The exergitic value of throttling ranged between (90-93) % due to the small surface area, which leads to low heat transfer losses.
Fig. 15 shows the relation between the evaporator exergy with different sizes of condensers at different temperatures 25℃, 30℃ and 35℃. The exergy value of the evaporator is around 98 %.
Fig. 16 shows the relation between the condenser heat rejections with different sizes of condensers at different ambient temperatures 25℃, 30℃ and 35℃. The condenser heat dissipation for refrigerant increases slightly with the increase in condenser size. The amount of refrigerant heat needed to reject is 140W to 185W at different ambient temperatures, while the air absorbing capacity is between 70W to 90W.
Fig. 17 shows the relation between the condenser heat transfer coefficients with different sizes of condensers at different ambient temperatures 25℃, 30℃ and 35℃. The value of the average heat transfer coefficient remained constant for different sizes of condensers due to the heat to be rejected is 140W to 185W as shown in **Fig. (19).** The values illustrated in the figure are the average value of superheat, saturated and subcooled regions depend on the length need to dissipate heat.
Fig. 18 shows the relations between the effectiveness of the condenser with different sizes of condensers at different ambient temperatures 25℃, 30℃ and 35℃. The effectiveness value of the condenser increases with the increase in the condenser size at each ambient temperature.
Fig. 19 shows the relation between the condenser thermal conductance with different sizes of condensers at different ambient temperatures 25℃, 30℃ and 35℃. The thermal conductance of the condensers increases due to the increase in the heat transfer area, while the evaporator remains constant because no change was done. The thermal conductances for condenser and evaporator were equal at condenser with leg 12, while the condenser thermal capacity is nearly three times the evaporator capacity at the point where the inner surface area is equal.
Fig. 20 shows the relation between the condenser area to total area ratio and allocation xi at 25℃ ambient temperature. At allocation 0.5 the χUA_c equal χUA_e when the area of the condenser is equals approximately 0.3 of the total area, and also at allocation 0.5 the χA_{ie} equal χA_{ic}, but when condenser equals 0.5 of the total area. It was found from **Fig. 12** for the relation between compressor exergy at different sizes of condensers, the best is at the condenser size between 13 legs and 15 legs. That means for optimum design, the condenser thermal capacity must be larger than the evaporator thermal capacity by (25-30) %, which is necessary in matching the components of the vapor compression refrigeration system design. The same results were found at 30℃ and 35℃.
Fig. 21 shows the relation between the irreversibility with different sizes of condensers at different ambient temperatures 25℃, 30℃ and 35℃. The irreversibility range of the cycle is about 0.097 to 0.137, while the highest irreversibility value of the cycle is for 25℃ followed be 30℃ and 35℃.
Fig. 22 shows the relation between the cycle exergy efficiency with different sizes of condensers at 25℃, 30℃ and 35℃ ambient temperatures. The highest value of exergy efficiency was at 25℃ ambient temperature at each condenser size, followed by 30℃ and 35℃.

6. CONCLUSIONS

The main objective of this work was to find the optimum working point with the lower irreversibility of a vapor compression refrigeration system for a domestic refrigerator. This was done using different sizes of condensers at different ambient temperatures with an exergy

analysis of the cycle components. A thermodynamic model for a steady state vapor compression refrigeration system for a domestic refrigerator working with R-134a has been developed depending on the EES software. The model validation was checked against the experimental results and the following concluding remarks are drawn from the model and tests:

1. The compressor has the largest exergy dissipation compared to other components of the cycle with an exergy efficiency of 25%.
2. The throttling device is the second in exergy dissipation after the compressor with 92% exergy efficiency.
3. The condenser exergy dissipation is higher than the evaporator with 93% exergy efficiency.
4. The evaporator has the lowest exergy dissipative with 98% exergy efficiency.
5. The optimum working condition can be obtained when the condenser thermal conductance is larger than the evaporator thermal conductance by (25-30) %. The design of the system must be carried out according to thermal conductance, rather than the internal surface area because; the point of equal inner area gave the worse working conditions.

REFERENCES:

- A. S. H. R. A. E Fundamental, 1997, *ASHRAE Handbook*. ASHRAE, Atlanta.
- Bejan, A., 1989, *Theory of Heat Transfer-Irreversible Refrigeration Plants*. International Journal of Heat and Mass Transfer, Vol. 32, No. 9, PP. 1631–1639.
- Bejan, A., 1996, *Entropy Generation Minimization*. CRC Press, New York.
- Bejan, A., 2006, *Exergy Analysis, Entropy Generation Minimization, and the Constructal Law*. Mechanical Engineers' Handbook.
- Chang, T. B., 2006, *Internal Irreversibility Analysis and Optimization of a Refrigeration Plant*. Jsme International Journal Series B-Fluids and Thermal Engineering, Vol. 49, No. 4, PP. 1260–1265.
- Hajal, J. El, Thome, J. R., & Cavallini, A., 2003, *Condensation in Horizontal Tubes, Part 1 : Two-Phase Flow Pattern Map*, Vol. 46, PP. 3349–3363.
- Holman, J. P, 2010, *Heat Transfer, Textbook*, 758.
- Incropera, Dewitt, Bergham and Lavibne, 2010, *Introduction to Heat Transfer. Fifth Edition*, John Wiley and Sons Inc., USA, CH.9, Page 535.
- Kandlikar, S.G., 1990, *A General Correlation For Saturated Two-Phase Flow Boiling Heat Transfer Inside Horizontal And Vertical Tubes*. ASME, Journal of Heat Transfer, February, Vol. 112, Pp. 219-228.
- Klein, S. A., & Reindl, D. T., 1998, *The Relationship of Optimum Heat Exchanger Allocation and Minimum Entropy Generation Rate for Refrigeration Cycles*. Journal of Energy Resources Technology, Vol. 120, No. 2, PP. 172-178.
- Khan, N., Khan, M., Ashar, M., & Khan, A. Z., 2015, *Energy and Exergy Analysis of Vapor Compression Refrigeration System with R12, R22, R134a*, Vol. 5, No. 3, PP. 210–216.
- Munson, B. R., Young, D. F., & Okiishi, T. H., 2006, *Fundamentals of Fluid Mechanics*, John Wiley & Sons. Inc., USA.
- Prakash, U., Vijayan, R., & Vijay, P., 2016, *Energy and Exergy Analysis of Vapor Compression Refrigeration System with Various Mixtures of HFC/HC*, International Journal of Engineering Technology, Management and Applied Sciences, Vol. 1, No. 4, PP. 40-48.
- Roy, R., & Mandal, B. K., 2014, *First Law and Second Law Analysis of Mechanical Vapor Compression Refrigeration System Using Refrigerants CFC12, R134a and R290*,

International Journal of Current Engineering and Technology, Special Issue.3, PP.191-195.

- Stanciu, C., Gheorghian, A., Stanciu, D., & Dobrovicescu, A., 2011, *Exergy Analysis and Refrigerant Effect on the Operation and Performance Limits of a One Stage Vapor Compression Refrigeration System*. Termotehnica, Vol. 1, PP. 36–42.
- Traviss, D.P., 1972, *Condensation in Refrigeration Condensers*. PhD Thesis, Massachusetts Institute of Technology, February.
- Thome, J. R., Hajal, J. El, & Cavallini, A., 2003, *Condensation in Horizontal Tubes, Part 2 : New Heat Transfer Model Based on Flow Regimes*, Vol. 46, PP. 3365–3387.
- Ukey R., Chaudhary S., 2012, *Exergy Analysis of Domestic Refrigerator with Different Refrigerants*, International Journal of Scientific and Engineering Research, Vol. 3, PP. 416 - 421.

NOMENCLATURE

Symbol	Definition	Unit
A	area	m^2
A_c	condenser area	m^2
$A_{contact}$	the contact area between the fins and tubes	m^2
A_e	evaporator area	m^2
A_f	suthe rface area of the fins	m^2
A_s	surface area	m^2
A_t	suthe rface area of the tubes	m^2
A_{tot}	total heat transfer area of the air-side (Afins+ At)	m^2
a	Kays & London power coefficient	
Bo	nucleate boiling number	
b	Kays & London power coefficient	
C	thermal capacitance	ṁ · Cp kW/K
C^*	thermal capacitance ratio Cmin/Cmax	
C_p	specific heat at constant pressure	kJ/kg.K
ED	exergy destruction	W
Ex	exergy	W
Fr	Froude number	
f	friction factor	
F_{1-2}	compressor shape factor	
G	total mass velocity of liquid and vapor	$kg/m^2.s$
g	gravitational acceleration	m/s^2
$H.E$	heat exchanger	
h_{fg}	latent heat	kJ/kg
h_n	enthalpy at state n (n=1,2,3 …)	kJ/kg
j	colburn j-factor (St.Pr2/3)	
k	thermal conductivity	W/m.℃
L	length of tube	m
m	mass flow rate	kg/s
Nu	Nusselt number	
NTU	number of transfer unit	
p	pressure	N/m^2
P	power	W
Pr	Prandtl number	
Q	heat transfer rate	W
Ra	Rayleigh number	
Re	Reynolds number	
r	radius	m
St	Stanton number	
S	entropy	kJ/kg.K
$\dot{S}$	entropy generation rate	kJ/kg.s
T	temperature	℃
t_f	fin thickness	m
UA	overall heat transfer coefficient	W/K
W	work	W
We	Weber Number	
x	quality or dryness fraction	

GREEK CHARACTERS

Symbol	Definition	Unit
α	heat transfer coefficient	W/m^2.°C
β	extend coefficient for air in natural convection	1/K
ϵ	emissivity	
Ɛ	effectiveness	
ε	void fraction	
δ	liquid film thickness	m
θ_{strat}	stratified anglerad	
ϵ_{scomp}	compressor surface emissivity	
μ	dynamic viscosity	N.s/m^2
η	efficiency	
η_f	fin efficiency	
η_s	air-side surface efficiency	
ρ	density	kg/m^3
σ	surface tension	N/m
σ_B	stefan-Boltzmann constant	W/m^2.k^4
ζ	exergy dissipation	
ξ	factor	
Λ	factor in Müller-Steinhagen and Heck correlation	

SUBSCRIPTS

Symbol	Definition
a	air
act	actual
amb	ambient
$comp$	compressor
$c.v$	control volume
dis	discharge
D	dimensionless
e	evap and evaporator
exp	expansion
ex	exergy
f	fin
i	in
l	liquid state
o	out
v	vapor
$wi-sat$	inside wall saturation region
c	cond and condenser
$cin-sat$	condenser inlet saturation
$cout-sat$	condenser outlet saturation
r	refrigerant
s	surface
sat	saturation
sub	sub-cool
sh	super-heat
$strat$	stratified
suc	suction
tot	total
tp	two phase
t	tube
Π	second
w	wall

Table 1. Values of constants for equation (13).

Type of flow	a	b
Laminar Re < 3500	1.10647	-0.78992
Transition 3500 < Re < 6000	$3.5194*10^{-7}$	1.03804
Turbulent Re > 6000	0.2243	-0.385

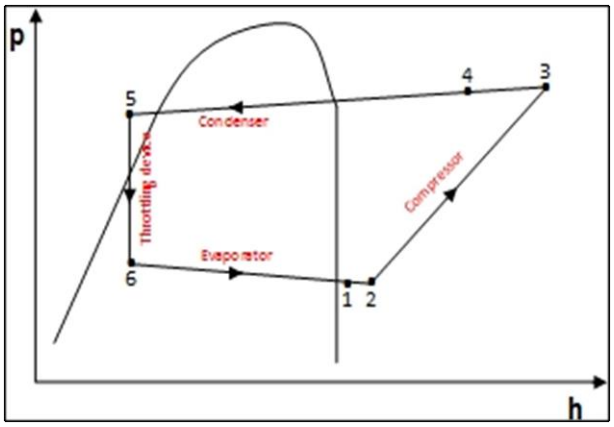

Figure 1. The P-h diagrams for vapor compression refrigeration cycle.

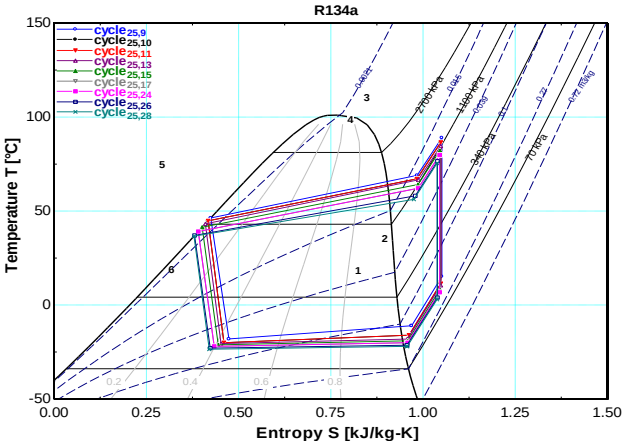

Figure 2. T-s diagrams of vapor compression refrigeration cycle with different sizes of condensers at 25°C

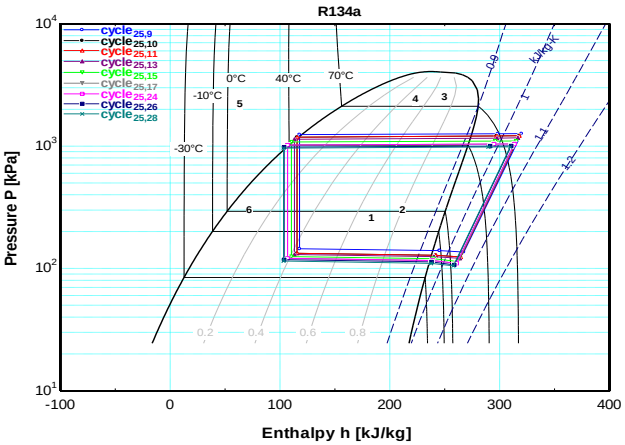

Figure 3. P-h diagrams of vapor compression refrigeration cycle with different sizes of condensers at 25°C

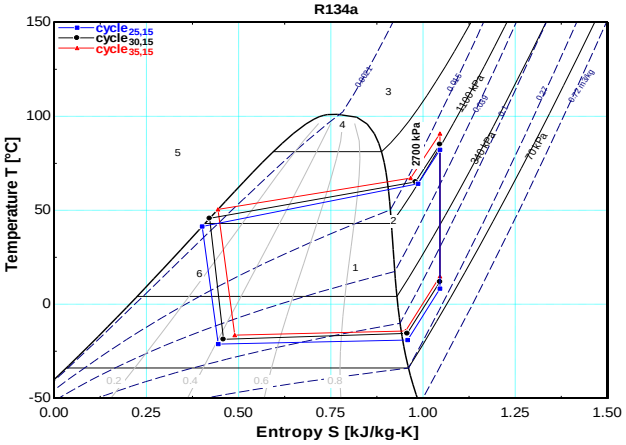

Figure 4. T-s diagrams of vapor compression refrigeration cycle for 15 legs condenser at 25°C, 30°C and 35°C ambient

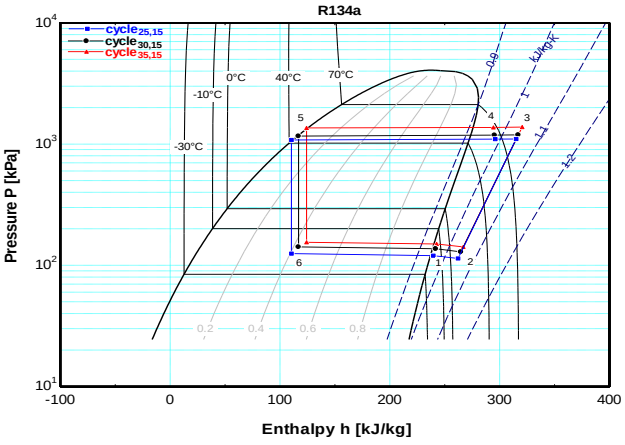

Figure 5. P-h diagrams of vapor compression refrigeration cycle for 15 legs condenser at 25°C, 30°C and 35°C ambient

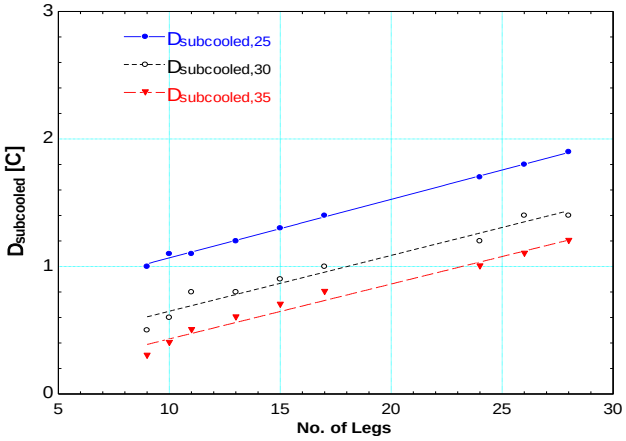

Figure 6. Subcooled degree via different sizes of condensers at 25°C, 30°C and 35°C ambient temperatures.

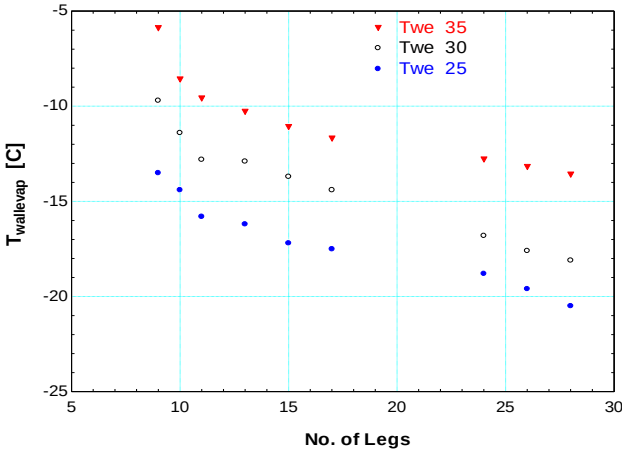

Figure 7. Evaporator wall temperature via different sizes of condensers at 25℃, 30℃ and 35℃ ambient temperatures.

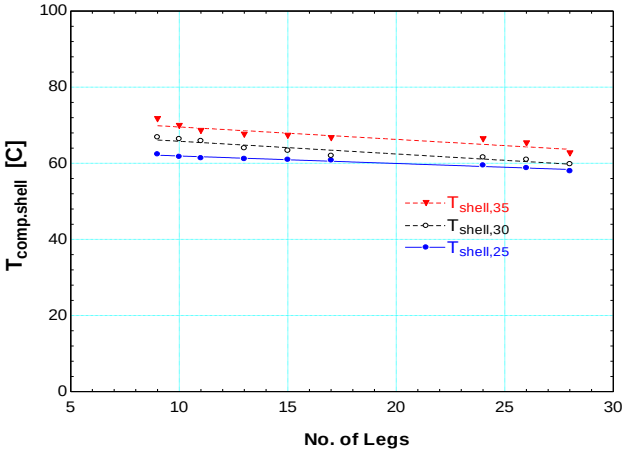

Figure 8. Compressor surface temperature via different sizes of condensers at 25℃, 30℃ and 35℃ ambient temperatures.

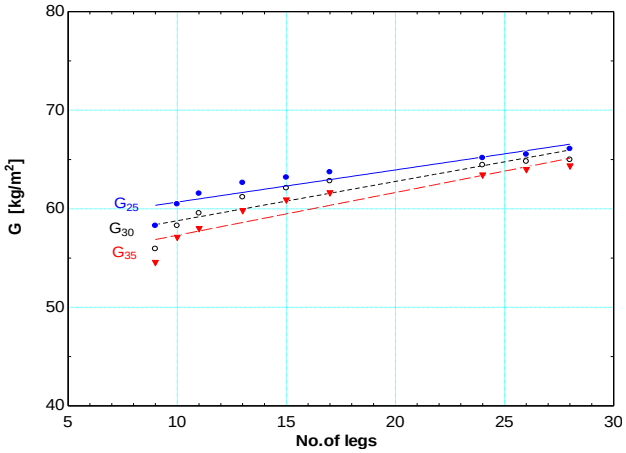

Figure 9. Mass velocity via different sizes of condensers at 25℃, 30℃ and 35℃ ambient temperatures.

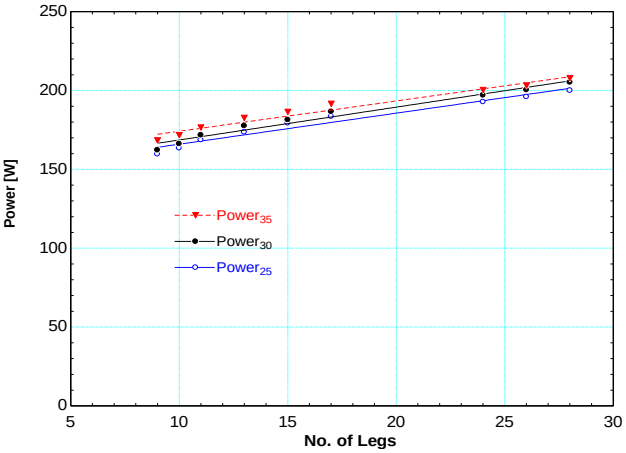

Figure 10. Power via different sizes of condensers at 25℃, 30℃ and 35℃ ambient temperatures.

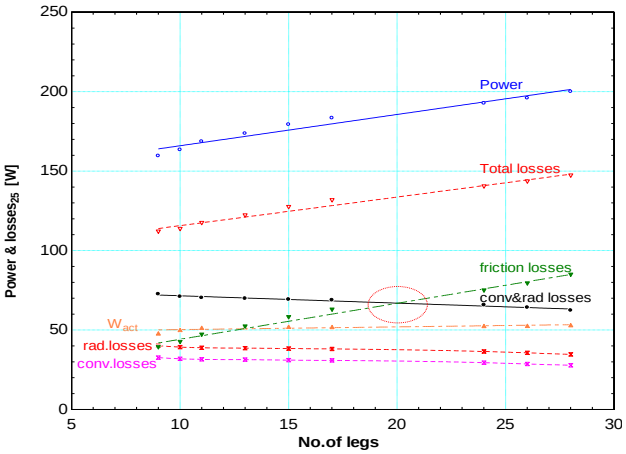

Figure 11. Total power consumption and the losses via different sizes of condensers at 25℃ ambient temperature.

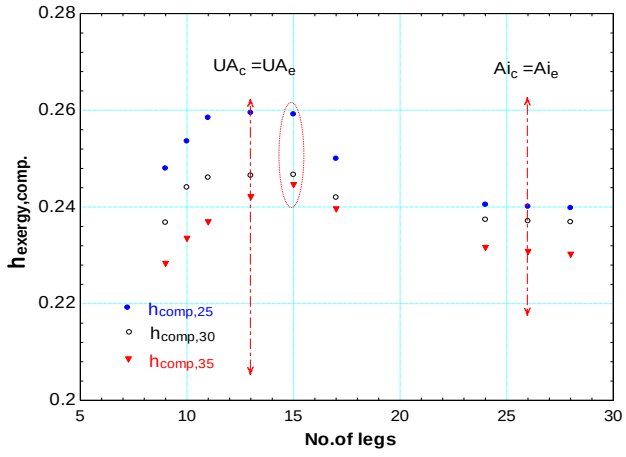

Figure 12. Exergy of compressor via different sizes of condensers at 25℃, 30℃ and 35℃ ambient temperatures.

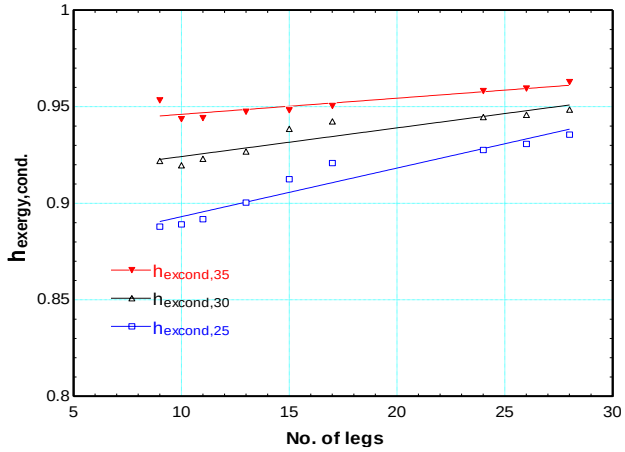

Figure 13. Condenser exergy via different sizes of condensers at 25℃, 30℃ and 35℃ ambient temperatures.

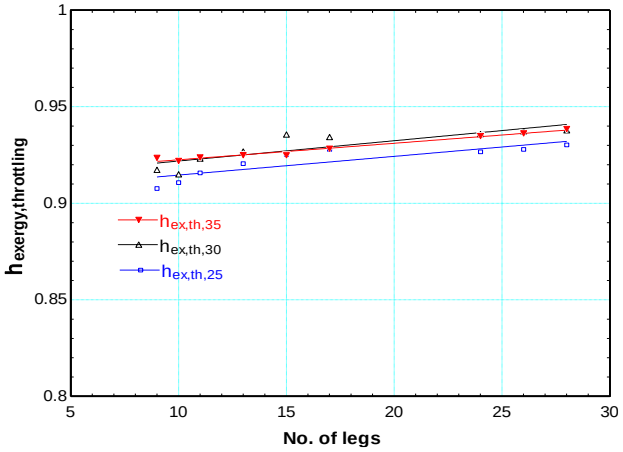

Figure 14. Throttling exergy via different sizes of condensers at 25℃, 30℃ and 35℃ ambient temperatures.

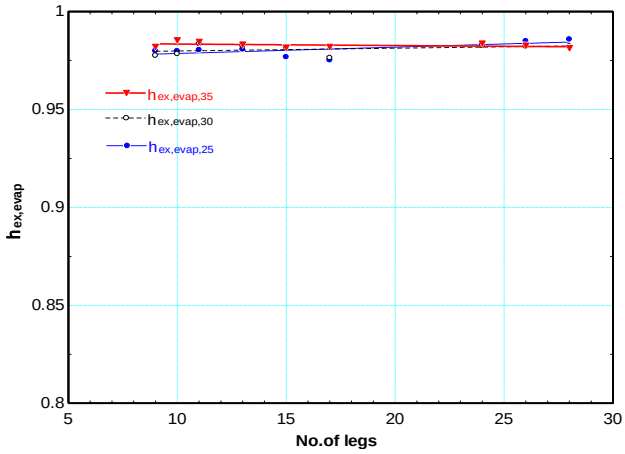

Figure 15. Evaporator exergy via different sizes of condesners at 254℃, 30℃ and 35℃ ambient temperatures.

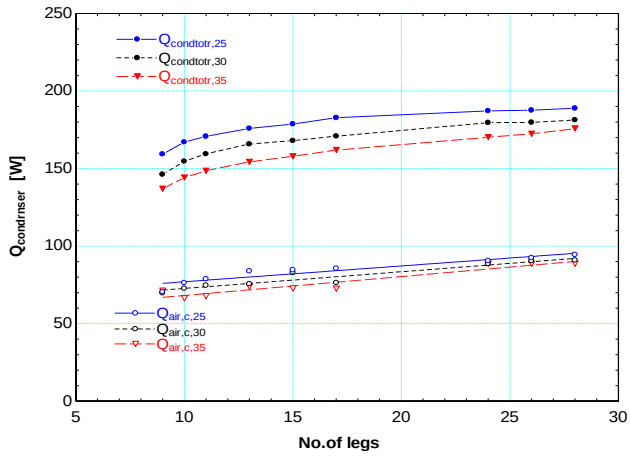

Figure 16. Condenser heat rejection via different sizes of condensers at 25℃, 30℃ and 35℃ ambient temperatures.

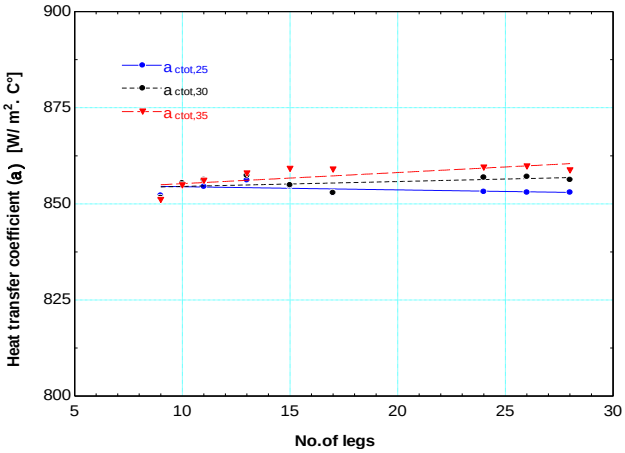

Figure 17. Condenser heat transfer coefficient via different sizes of condensers at 25℃, 30℃ and 35℃ ambient

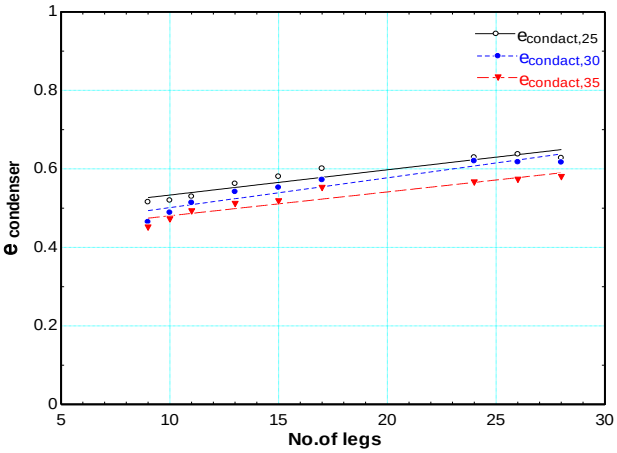

Figure 18. Effectiveness of condenser via different sizes of condensers at 25℃, 30℃ and 35℃ ambient temperatures.

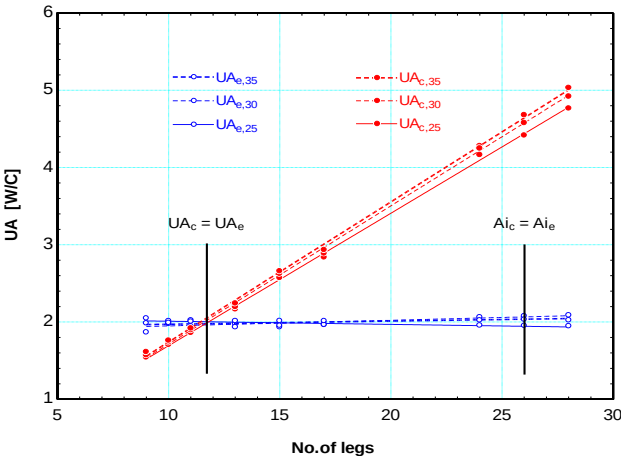

Figure 19. Thermal capacity via different size of condenser at 25℃, 30℃ and 35℃ ambient temperatures.

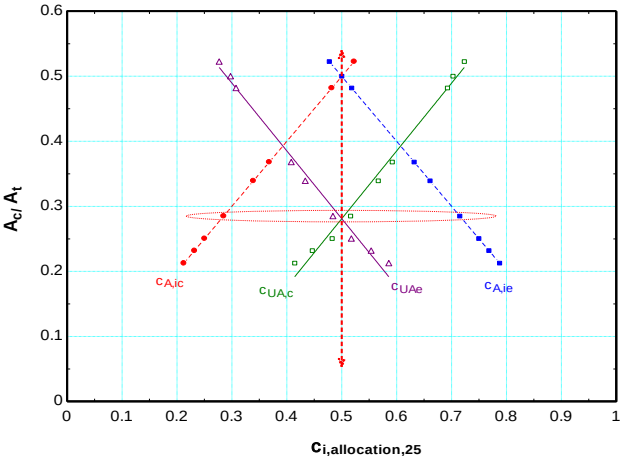

Figure 20. The percentage of condenser area (condenser + evaporator) to total area ratio with allocation xi at 25℃ ambient temperature.

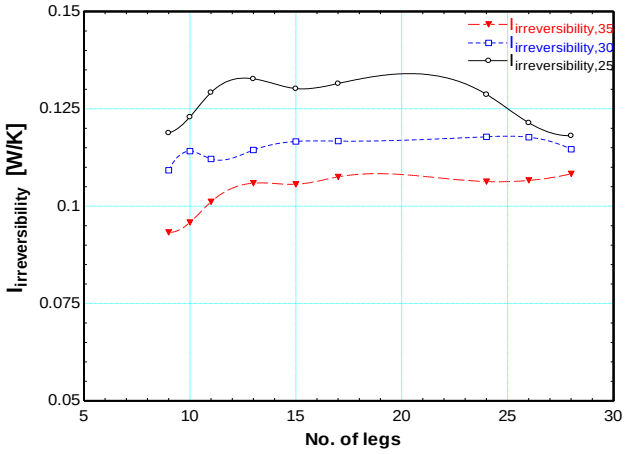

Figure 21. Irreversibility via different size of condenser at 25℃, 30℃ and 35℃ ambient temperatures.

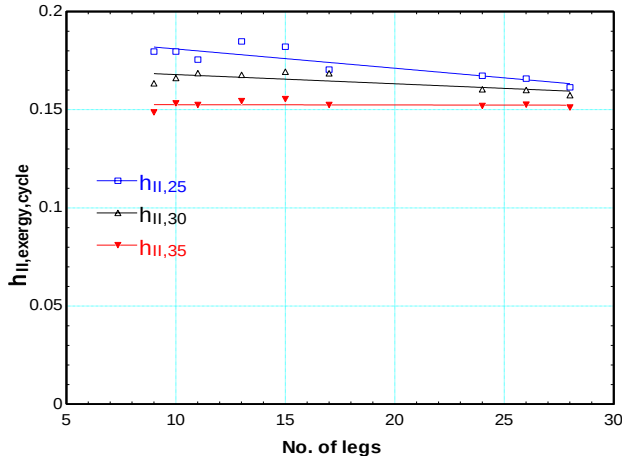

Figure 22. Second law efficiency of the cycle via different sizes of condensers at 25℃, 30℃ and 35℃ ambient temperatures.